Temperature Dependent Performance of ITO Schottky Contacts on β- Ga_2O_3

Xinyi Xia[1], Minghan Xian[1], Chaker Fares[1], Fan Ren[1], Marko Tadjer[2] and S. J. Pearton [3]

[1]Department of Chemical Engineering, University of Florida, Gainesville, FL 32611, USA

[2]Naval Research Laboratory, Washington DC 20375, USA

[3]Department of Materials Science and Engineering, University of Florida, Gainesville FL 32611, USA

Abstract

Sputtered ITO was used as a rectifying contact on lightly n-type (n~10^{16} cm^{-3}) β- Ga_2O_3 and found to exhibit excellent Schottky characteristics up to 500K, with no thermally-driven degradation to this temperature. The barrier height extracted from current-voltage characteristics was 1.15±0.04 eV at 300K and 0.78±0.03 eV at 500K, with thermionic behavior of charge carriers over the image force lowered Schottky barriers dominating the carrier transport at low temperatures. The breakdown voltages were 246, 185 and 144 V at 300, 400 and 500K, respectively. At 600K, the diodes suffered irreversible thermal damage. The diode on/off ratio was >10^5 for reverse biases up to 100V. At higher reverse voltage, the current shows an $I \propto V^n$ relationship with voltage, indicating a trap-assisted space-charge-limited conduction (SCLC) mechanism. We observed this SCLC relation when the reverse voltage was larger than 100 V for 300 K and 400 K and at <100V at 500K. The ITO can also be used to make Ohmic contacts on heavily doped Ga_2O_3 suggesting the possibility of completely optically transparent power devices.

Introduction

There are two particular polytypes of Ga_2O_3 that are attracting interest for high power transistors and rectifiers and solar-blind UV photodetectors [1-6]. The α-polytype has a larger bandgap and a hexagonal crystalline structure (in contrast to the low-symmetry monoclinic structure of the β-phase) the same as of sapphire (α-Al_2O_3) and so it has a better lattice matching to α-Al_2O_3 substrates. This facilitates improvement of the epilayers structural quality. The β-polytype is available in melt-grown bulk form, with controllable n-type doping, and is the most stable form [1-3]. The high breakdown field of this wide bandgap semiconductor has enabled many demonstrations of vertical and lateral rectifiers with reverse breakdown voltages in the kV range of interest for electric vehicle (EV) charging stations, power management in residential solar systems and battery energy storage systems [7-29]. In particular, the transition to fast EV charging stations equipped with advanced DC chargers is accelerating -the state of the art is that currently a DC charger with 150 kW can put a 200 km charge on an EV in ~15 minutes [30,31]. For most low-voltage urban applications, breakdown voltages of 1.2 kV suffices. The high breakdown field of Ga_2O_3 enables greater voltage blocking capability and lower conduction losses due to a lower on-resistance reduction in comparison with Si-based devices [3,4,9,30].

A crucial aspect of these high-power rectifiers are the Schottky contacts. These contacts need to be thermally stable, the interface between the metal and the Ga_2O_3 needs to be of high quality so that any defect-related leakage current is insignificant and finally, the largest barrier height is needed if the maximum electric field is to be reached [32-42]. Li et al.[29] calculated that to reach the intrinsic breakdown electric field in Ga_2O_3, the barrier height of the Schottky contact would \need to be of the order of 2.2 -3 eV. These values have not been reached with any of the metals examined to date, with the highest values of ~2.1 eV reported for oxidized metal contacts

of PtO_x and IrO_x deposited by reactive sputtering on (-201) Ga_2O_3 substrates [37,41]. In high-power Schottky rectifiers, the largest barrier is needed to reach the maximum electric field (2.2-3eV in the case of Ga_2O_3). However, in power-rectifiers if the barrier height is too high, the forward voltage drop at the targeted current will be also high, thus leading to a high power dissipation, so that striving for the highest barrier height is not always desirable. Previous work has shown that the orientation of the Ga_2O_3 has a strong influence on whether there is a correlation of barrier height with metal work function [32,33]. Lyle et al.[32] showed that (100) surfaces showed the strongest correlation, while (-201) and (101) had stronger Fermi level pinning effects, due to the differences in dangling bond densities [32].

In this work, we describe the performance of sputtered ITO contacts on (100) Ga_2O_3, as a function of temperature up to 500K. Transparent gates would also facilitate probing of single event radiation upsets using x-ray excitation sources [44]. They may also be useful in limited types of optically-triggered Ga_2O_3 power devices if a gap state is employed, since the bandgap of ITO is around 4 eV and that of Ga_2O_3 is larger. Optically-triggered power management devices use optical control to avoid the thermal degradation of the gate electrode when used at high temperature and there is complete electrical isolation between the low-voltage controller and HV power stages [43]. An all optically-controlled gate would add flexibility to thyristor designs, allowing them to be used to their full potential.

Thin (10nm) sputtered indium tin oxide (ITO) has been employed previously as an intermediate layer between Ti/Au and heavily doped (-201) β-Ga_2O_3 to enhance formation of an Ohmic contact upon annealing at 400-600°C [45,46]. The band alignment of ITO on Ga_2O_3 under those conditions is favorable for electron injection, with a conduction band offset of -0.32 eV

[45,46]. However, in the as-deposited state on lightly doped Ga_2O_3 and for anneal temperatures up to 500K, we find the ITO to provide a rectifying contact.

Experimental

The drift region of the material consisted of a 10 μm thick, lightly Si doped epitaxial layer grown by halide vapor phase epitaxy (HVPE) with carrier concentration of 3×10^{16} cm^{-3}, and this epitaxial layer was grown on a (001) surface orientation, 2-inch diameter Sn-doped ($n=10^{19}$ cm^{-3}) β-Ga_2O_3 single crystal (Novel Crystal Technology, Japan). The HVPE layer was actually grown initially to a thickness of ~ 20 μm, but then chemically mechanically polished to planarize the surface by removing ~10 μm of material. The wafer surfaces were ultrasonically cleaned in acetone, methanol, and isopropyl alcohol.

A full area Ti/Au backside Ohmic contact was formed by e-beam evaporation and was annealed at 550 ̊C for 30s under N_2 ambient. After backside Ohmic formation, the front of the sample was cleaned using HCl and then treated with ozone for 20 minutes to remove residual hydrocarbons. Next, the sample was patterned for Schottky contact formation. A 100 nm ITO layer was deposited by dc sputtering at room temperature using a 3-in. target of ITO. The dc power was 125 W and the process pressure was 5 mTorr in pure Argon ambient. Edge termination was not used, in order to focus on the ITO contact characteristics free of any edge effects. Figure 1 shows a schematic of the competed devices, with circular contact diameters of 50-200 μm and square contacts of length 400μm. There was no clear dependence of forward and reverse current densities over the range of contact sizes investigated. Figure 2 shows an optical microscope image and contact geometry of the fabricated diodes.

The current-voltage (I-V) characteristics were recorded over the temperature range 300-500K on a temperature-controlled stage. Forward current measurements were recorded with a

HP 4156 parameter analyzer. No hysteresis was observed in any of the rectifier characteristics. Reverse currents were measured with a Tektronix 370-A curve tracer. We measured 4-5 different diodes for each condition, with the results being within 5% within this distribution. The forward direction was dominated by the thermionic emission (TE) current over most of the temperature range, while in the reverse direction, the thermionic field emission (TFE) and tunneling currents played an important role at high reverse bias. To extract the zero-bias equivalent barrier height (Φ_b) and ideality factor (n), we used the relationship for current density in TE theory, given by [32,46,47]

$$J = J_0 \exp(eV_A/nkT)\,[1-\exp(-eV_A/kT)]$$

where $J_0 = A^* m_{eff}/m_0 T^2 \exp(\Phi_B/kT)$, e is electronic charge and A^* is the Richardson constant (33.7 $A.cm^{-2}K^{-2}$) and V_A is the bias voltage applied. The values of barrier height were corrected for the image force (IF) lowering, as described elsewhere and also represent the average of 4-5 different diodes at each condition. [41]. Capacitance-Voltage (C-V) characteristics were recorded with an Agilent 4284A Precision LCR Meter to conform the carrier concentration in the epi layer. The diode on/off ratio is another figure-of-merit was measured when switching from 3V forward to reverse biases up to 100V. The reverse breakdown voltage was defined as the bias for a reverse current reached before 3mA.

Results and Discussion

Figure 3 shows the forward current density for the 100 μm diameter circular diodes as a function of temperature. The devices were sequentially measured at increasing temperatures up to 500K, then returned to 300K and re-measured. For these temperature cycled diodes, the junction diameter is 500 micrometer, which converts to an increase in junction current of about 2 nA ($2x10^{-9}$ A) after the heating cycle to 500 K. However, a change of nA in current densities

many orders higher is not sufficient to draw the conclusion the samples are not thermally stable after that cycling. Small shifts in forward turn-on voltage can result from changes in on-resistance or barrier height. As stated earlier, there was no difference in current density as a function of contact size or geometry. The carrier concentration in the epi layer did not change as a result of the thermal cycling as determined by C-V measurements, indicating that compensating Ga vacancies or other defects were not created at these temperatures. The on-state resistance of the rectifiers, R_{ON}, was 12 mΩ.cm^2 at 300K and 29 mΩ.cm^2 at 500K. At 600K, the diodes suffered irreversible thermal damage.

The zero bias effective barrier height and ideality factors were extracted from the linear portion of the forward bias characteristics through the correction factor $[eE/4\pi\varepsilon]^{0.5}$, where E is the electric field at the ITO/Ga_2O_3 interface and ε is the dielectric constant of the semiconductor [41]. The results are shown as a function of temperature in Figure 4. The barrier height decreases monotonically with increasing temperature, while the ideality factor increases. This is commonly observed for contacts on Ga_2O_3 [32, 33,37,39]. However, in many cases [34-36,38,40,41] the behavior of n and barrier height is exactly opposite, i.e. n decreases with temperature (tending to one) and barrier height increases with temperature. This can be due to the presence of other conduction mechanisms and also contact inhomogeneity. Another notable exception is the large thermally activated increase in the barrier height for Pd Schottky contacts occurring between 250-450 °C when heated in air [41]. This change was ascribed to the oxidation of the Pd metal layers, creating higher barrier height PdO_x regions. The high ideality factor above ~400 K indicate other current transport mechanisms are present as the barrier is lowered.

If the Mott-Schottky relationship holds for ITO on (100) Ga_2O_3, the expected barrier height would be 0.75 eV from the difference in energy between the metal work function of 4.8

eV [47] and the electron affinity of Ga_2O_3 of 4.05 eV. This is not an unreasonable assumption given the high degree of ionicity of the bonds in Ga_2O_3 [32]. However, the experimental value of 1.15 eV at room temperature is larger than this prediction, suggesting that additional factors are determining the effective barrier height and is certainly larger than expected from contact inhomogeneity considerations. The SBH can be dependent on the surface orientation of Ga_2O_3, Lyle et al.[32] have made investigations of different metals on different orientations of Ga_2O_3 found that the change of barrier height with metal work function can be used as a useful measure of the applicability of the Mott-Schottky relationship. In Figure 5, we plot previously reported values [32] for Ti, Mo, Co and Ni on (100) Ga_2O_3 with the experimental value for ITO determined in this work for (001) orientation, which are the two surfaces with highest stability [48]. Thus we feel a comparison is more likely to be valid relative to results on the other orientations. There is an extensive discussion of this by Lyle et al. [32]. The straight line is to guide the eye and not to explicitly evaluate the presence of Fermi level pinning.

Overall, there is a positive correlation between Schottky barrier heights and the work function of the metal contacts for these orientations and the experimental value for ITO on the (001) orientation fits well with previous results for the other metals on the (100) orientation, the other stable surface [32]. This is in contrast to contacts on (-201) and (010) β-Ga_2O, which exhibited little or mixed correlation between these parameters [32,49]. In the case of (-201) surfaces, the higher density of O dangling bonds was proposed to explain the strong Fermi level pinning on this surface [32]. Harada et al. [48] employed a novel layered $PdCoO_2$ contact on Ga_2O_3 to achieve a barrier height of 1.8eV, well above that expected from the Mott-Schottky relation. This significantly expands the temperature range for achieving good rectification ratios [48]. It is clear in the case of ITO on (001) Ga_2O_3 that Fermi level pinning is present.

Figure 6 shows the reverse current density characteristic as a function of temperature. The breakdown voltages were 246, 185 and 144 V at 300, 400 and 500K, respectively, showing that impact ionization is not the breakdown mechanism, since that should exhibit positive temperature coefficient. It is common for new technologies like Ga_2O_3 to exhibit defect-dominated behavior in the early stages of development, as was observed with both SiC and GaN [1,9]. There was also no significant change in current density at room temperature as a result of the thermal cycling to 500K. The variation in reverse current densities as a function of temperature were within the experimental variation from diode-to-diode of ~10%.

The on-off ratio is another figure of merit is the figure of merit in that having high on-current and low leakage current in reverse bias is desirable. This was $>10^5$ for all temperatures measured, as shown in Figure 7.

As shown in Figure 8, at lower voltages, reverse bias leakage current density was dominated by thermionic field emission (TFE) , which is strongly dependent on ambient temperature. We have reported similar data previously for Ni/Au contacts on these types of rectifiers [47]. When higher reverse voltages are applied, electrons are injected into the drift region, and the current shows an $I \propto V^n$ relationship with the voltage, indicating a trap-assisted space-charge-limited conduction (SCLC) mechanism [49-53]. Under this mechanism, a current hump should be observed before the trap-filled limited voltage, and with electrons continue to be injected into the drift region, it will lead to a breakdown. The reverse current characteristics at different temperatures all show a $I \propto V^n$ relationship. The data fits a relationship $I \propto V^n$, where n is ~2-6.8, dependent on temperature. Trap-mediated SCLC should have n>2 [52]. In this higher field region, the space charge limited current is proportional to the product of electron saturation velocity times voltage divided by the electrode spacing. The value of n varies with the injection

level and is also related to the distribution of trapping centers. Values as high as 22 have been reported in GaN Schottky diodes with low densities of traps (10^{15} cm^{-3}) [53].

As mentioned earlier, the ITO can be used to enhance Ohmic contact formation on doped Ga_2O_3. Oshima et al.[54] found that sputter-deposited ITO electrodes became Ohmic contacts on n-type β-Ga_2O_3(010) substrates after rapid thermal annealing at 900–1150 °C. This raises the possibility of using ITO on both sides of vertical rectifier structures to make fully transparent power devices. An optical image of such a device is shown in Figure 9. The structure in this case is ITO top Schottky contact, epi Ga_2O_3, Ga_2O_3 substrate and ITO rear Ohmic contact. The optical transmittance was 83% at 360 nm and > 90% for 400-800nm without annealing, consistent with past reports [55]. We will conduct a more thorough study of the effect of annealing in future.

Summary and Conclusions.

ITO is shown to provide a rectifying contact to lightly doped (100) Ga_2O_3 up to temperatures of 500K. The barrier height at room temperature is 1.15 eV and fits a trend observed for metal contacts on the (100) orientation that correlated metal work function with the electron affinity of the semiconductor. The rectification ratio was $>10^5$ up to 500 K and the contacts appear useful for applications requiring optically transparent contacts. If more heavily doped substrates are used, the ITO can be made to behave as an Ohmic contact, perhaps assisted by an annealing step, and thus to the possibility of using transparent contacts on both sides of vertical rectifier structures arises. This allows realization of a fully transparent power device.

Data Availability Statement

All data that support the findings of this study are included within the article.

Acknowledgments

The work at UF was performed as part of Interaction of Ionizing Radiation with Matter University Research Alliance (IIRM-URA), sponsored by the Department of the Defense,

Defense Threat Reduction Agency under award HDTRA1-20-2-0002. The content of the information does not necessarily reflect the position or the policy of the federal government, and no official endorsement should be inferred. The work at UF was also supported by NSF DMR 1856662 (James Edgar). The work at NRL was supported by the Office of Naval Research.

References

1. E. Ahmadi and Y. Oshima, Materials issues and devices of α- and β-Ga_2O_3, J. Appl. Phys. 126, 160901 (2019)

2. Zbigniew Galazka, β-Ga_2O_3 for wide-bandgap electronics and optoelectronics, Semicond. Sci. Technol. 33, 113001 (2018).

3. S. J. Pearton, J. Yang, P. H. Cary, F. Ren, J. Kim, M. J. Tadjer, and M.A. Mastro, Appl. Phys. Rev., 5, 011301 (2018).

4. M.H. Wong and M. Higashiwaki, Vertical β-Ga_2O_3 Power Transistors: A Review, IEEE T. Electr Dev. 67, 3925 (2021).

5. L. A. M. Lyle, S. Okur, V. S. N. Chava, M. L. Kelley, R. F. Davis, G. S. Tompa, M. V. S. Chandrashekhar, A. B. Greytak, and L. M. Porter, J. Electron. Mater. 49, 3490 (2020).

6. X. Chen, F. Ren, S. Gu and J. Ye, Photon Res 7, 382 (2020).

7. N. Allen, Ming Xiao, Xiaodong Yan, Kohei Sasaki, Marko J. Tadjer, Jiahui Ma, Ruizhe Zhang, Han Wang and Yuhao Zhang, IEEE Electron Dev. L., 40, 1399 (2019).

8. K. Konishi, K. Goto, H. Murakami, Y. Kumagai, A. Kuramata, S. Yamakoshi, and M. Higashiwaki, Appl. Phys. Lett. 110, 103506 (2017).

9. S. J. Pearton, F. Ren, M. Tadjer, and J. Kim, J. Appl. Phys. 124, 220901 (2018).

10. Samuel James Bader, Hyunjea Lee, Reet Chaudhuri, Shimin Huang, Austin Hickman, Alyosha Molnar, Huili Grace Xing, Debdeep Jena, Han Wui Then, Nadim Chowdhury, Tomás Palacios, IEEE T. Electron Dev. 67, 4010 (2020).

11. Z. Hu, Hong Zhou, Qian Feng, Jincheng Zhang, Chunfu Zhang, Kui Dang, Yuncong Cai, Zhaoqing Feng, Yangyang Gao, Xuanwu Kang, Yue Hao, IEEE Electron Dev. L., 39, 1564 (2018).

12. W. Li, K. Nomoto, Z. Hu, D. Jena, and H. G. Xing, EEE Electron Dev. L., 41, 107 (2020).

13. W. Li, K. Nomoto, Z. Hu, T. Nakamura, D. Jena, and H. G. Xing, Single and multi-fin normally-off Ga_2O_3 vertical transistors with a breakdown voltage over 2.6 kV, in 2019 IEEE International Electron Devices Meeting (IEDM), Dec. 2019, p. 12.4.1-12.4.4.

14. M. Ji, Neil R. Taylo, Ivan Kravchenko, Pooran Joshi, Tolga Aytug, Lei R. Cao, M. Parans Paranthaman, IEEE T. Power Electr., 36, 41 (2021).

15. J.C. Yang, F. Ren, M.J. Tadjer, S.J. Pearton and A. Kuramata, ECS J. Solid State SC., 7, Q92 (2018).

16. Jiancheng Yang, Fan Ren, YenTing Chen, Yu Te Liao, Chin Wei Chang, Jenshan Lin, Marko J. Tadjer, S. J. Pearton and Akito Kuramata, J. Electron. Devices Soc. 7, 57 (2019).

17. Yangyang Gao, Ang Li, Qian Feng, Zhuangzhuang Hu, Zhaoqing Feng, Ke Zhang, Xiaoli Lu, Nanoscale Res. Lett.14, 8 (2019).

18. Z. Hu, Yuanjie Lv, Chunyong Zhao, Qian Feng Zhaoqing Feng, Kui Dang, Xusheng Tian, Yachao Zhang, Jing Ning, Hong Zhou, Xuanwu Kang, Jincheng Zhang and Yue Hao, IEEE Electron Dev. L., 4 441 (2020).

19. J. Yang, Minghan Xian, Patrick Carey, Chaker Fares, Jessica Partain, Fan Ren, Marko Tadjer, Elaf Anber, Dan Foley, Andrew Lang, James Hart, James Nathaniel, Mitra L Taheri, SJ Pearton, Akito Kuramata, Appl. Phys. Lett., 114, 232106 (2019).

20. C. Buttay, H.-Y. Wong, B. Wang, M. Xiao, C. DiMarino, and Y. Zhang, Microelectron. Reliab., 114, 113743 (2020).

21. Hongpeng Zhang, Lei Yuan , Xiaoyan Tang, Jichao Hu, Jianwu Sun, Yimen Zhang, Yuming Zhang and Renxu Jia, IEEE T. Power Electr. 35, 5157 (2020).

22. Ming Xiao, Boyan Wang, Jingcun Liu, Ruizhe Zhang, Student Zichen Zhang, Chao Ding, Shengchang Lu, Kohei Sasaki, Guo-Quan Lu, Cyril Buttay, and Yuhao Zhang, IEEE T. Power Electr. 6, 8565 (2021).

23. K. Sasaki, Daiki Wakimoto, Quang Tu Thieu, Yuki Koishikawa, Akito Kuramata, Masataka Higashiwaki and Shigenobu Yamakoshi, IEEE Electron Dev. L., 38, 783 (2017).

24. Q. He, Wenxiang Mu, Bo Fu, Zhitai Jia, Shibing Long, , Zhaoan Yu, Zhihong Yao, Wei Wang, Hang Dong, Yuan Qin, Guangzhong Jian, Ying Zhang, Huiwen Xue, Hangbing Lv, Qi Liu, Minghua Tang, Xutang Tao and Ming Liu, IEEE Electron Dev. L., 39, 556 (2018).

25. Z. Hu, Hong Zhou, Qian Feng, Jincheng Zhang, Chunfu Zhang, Kui Dang, Yuncong Cai, Zhaoqing Feng, Yangyang Gao, Xuanwu Kang , and Yue Hao, IEEE Electron Dev. L., 39, 1567 (2018)

26. Yuanjie Lv, Yuangang Wang, Xingchang Fu, Shaobo Dun, Zhaofeng Sun, Hongyu Liu, Xingye Zhou, Xubo Song, Kui Dang, Shixiong Liang, Jincheng Zhang, Hong Zhou, Zhihong Feng, Shujun Cai, and Yue Hao, IEEE T. Power Electr. (2020).

27. H.H. Gong, X. H. Chen, Y. Xu, F.-F. Ren, S. L. Gu, and J. D. Ye, Appl. Phys. Lett. 117, 022104 (2020).

28. Ribhu Sharma, Minghan Xian, Chaker Fares, Mark E. Law, Marko Tadjer, Karl D. Hobart, Fan Ren and S. J. Pearton, J. Vac. Sci. Technol. A 39, 013406 (2021).

29. Wenshen Li, Kazuki Nomoto, Debdeep Jena and Huili Grace Xing, Thermionic emission or tunneling? Appl. Phys. Lett. 117, 222104 (2020).

30. Javier Ballestín-Fuertes, Jesús Muñoz-Cruzado-Alba, José F. Sanz-Osorio and Erika Laporta-Puyal, Electronics, 10, 677 (2021).

31. Examples of the current state-of-the-art in EV charges can be found at several sites, eg. Fast EV Charging—Infineon Technologies. Available online: https://www.infineon.com/cms/en/applications/industrial/fastev-charging/

ABB. High Power Charging|High Power Fast Chargers|ABB. Available online: https://new.abb.com/ev-charging/products/car-charging/high-power-charging

Phoenix Contact High Power Charging—The Technology for Fast Charging Stations. Available online: https://www.phoenixcontact.com/online/portal/pi?1dmy&urile=wcm:path:/pien/web/main/products/technology_pages/ subcategory_pages/High_power_charging/b1c8a245-f088-4fad-b144-cea31e7f9a82

32. Luke A. M. Lyle, Kunyao Jiang, Elizabeth V. Favela, Kalyan Das, Andreas Popp and Zbigniew Galazka, Guenter Wagner, and Lisa M. Porter, J. Vac. Sci. Technol. A 39, 033202 (2021).

33. Lisa M. Porter and Jenifer R. Hajzus, Journal of Vacuum Sci. Technol. A 38, 031005 (2020).

34. T.-H. Yang, H. Fu, H. Chen, X. Huang, J. Montes, I. Baranowski, Kai Fu and Yuji Zhao, J. Semicond. 40, 012801 (2019).

35. E. Farzana, Z. Zhang, P. K Paul, A. R Arehart, and S. A. Ringel, Appl. Phys. Lett., 110, 2017.

36. Z Jian, S Mohant and E Ahmadi, Appl. Phys. Lett. 116, 152104 (2020).

37. C. Hou, K. R. York, R. A. Makin S. M. Durbin, R. M. Gazoni, R. J. Reeves and M. W. Allen, Appl .Phys. Lett. 117, 203502 (2020).

38. S. Ahn, F. Ren, L. Yuan, S. J. Pearton, and A. Kuramata, ECS J. Solid State SC 6, P68 (2017).

39. M. Higashiwaki, Keita Konishi, Kohei Sasaki, Ken Goto, Kazushiro Nomura, Quang Tu Thieu and Rie Togashi, Appl. Phys. Lett. 108, 133503 (2016).

40. M. Xian, C. Fares, F. Ren, B. P. Gila, Y.-T. Chen, Y.-T. Liao, M. Tadjer and S. J. Pearton, J. Vac. Sci. Technol. B 37, 061201 (2019).

41. Caixia Hou, Rodrigo M. Gazoni, Roger J. Reeves and Martin W. Allen, IEEE T Electron Dev, 68, 1791 (2021).

42. Wenshen Li, Devansh Saraswat, Yaoyao Long, Kazuki Nomoto, Debdeep Jena and Huili Grace Xing, Appl. Phys. Lett. 116, 192101 (2020).

43. Srikanta Bose and Sudip K.Mazumde, Solid State Electron 62, 5 (2011).

44. A. Khachatrian, N.J.H. Roche, S.P. Buchner, A.D. Koehler, T.J. Anderson, D. McMorrow, S.D. Lalumondiere, J.P. Bonsall, E.C. Dillingham, D.L. Brewe, IEEE T. Nucl. Sci. 66, 368 (2019).

45. P.H. Carey IV, F. Ren, D.C. Hays, B.P. Gila, S.J. Pearton, S. Jang and A. Kuramata, Appl. Surf. Sci. 422, 179 (2017).

46. Patrick H. Carey IV, Jiancheng Yang, Fan Ren, D. C. Hays, S. J. Pearton, Akito Kuramata and Ivan I Kravchenko , J. Vac. Sci. Technol. B. 35, 061201 (2017).

47. Y. Park, V. Choong, Y. Gao, B.R. Hsieh, C.W. Tang, Appl. Phys. Lett. 68, 2699 (1996).

48. T. Harada, S. Ito and A. Tsukazaki, Sci Adv 5, eaax5733 (2019).

49. Xinyi Xia, Minghan Xian, Patrick Carey1, Chaker Fares, Fan Ren, Marko Tadjer, S. J. Pearton, Thieu Quang Tu, Ken Goto and Akito Kuramata, J. Phys. D: Appl. Phys. 54, 305103 (2021).

50. P. Mazzolini, A. Falkenstein, C. Wouters, R. Schewski, T. Markurt, Z. Galazka, M. Martin, M. Albrecht and O. Bierwagen, APL Mater. 8, 011107 (2020).

51. M. Xiao, Tomás Palacios and Yuhao Zhang, Appl. Phys. Lett. 114, 163503 (2019).

52. M. A. Lampert and P. Mark, Current Injection in Solids (Academic Press, New York, 1970).

53. X.M. Shen, D.G. Zhao, Z.S. Liu, Z.F. Hu, H. Yang and J.W. Liang, Solid State Electron 49, 847 (2005).

54. T. Oshima, R. Wakabayashi, M. Hattori, A. Hashiguchi, N. Kawano, K. Sasaki, T. Masui, A. Kuramata, S. Yamakoshi, K. Yoshimatsu, A. Ohtomo, T. Oishi and Makoto Kasu, , Jpn. J. Appl. Phys. 55 1202B7 (2016).

55. Liu Jianjun, Yan Jinliang, Shi Liang and Li Ting, J. Semicond, 31, 103001 (2010).

Figure Captions

Figure 1. Schematic of layer structure of vertical rectifier used in this work.

Figure 2. Optical microscope image of Schottky contact layout.

Figure 3. Forward J-V characteristics as a function of temperature for ITO Schottky contacts on (100) β-Ga_2O_3. The diameter of each diode is 500 μm.

Figure 4. Extracted zero-bias barrier heights and ideality factors for ITO contacts, assuming thermionic emission dominates, as a function of temperature.

Figure 5. Comparison of experimental and theoretical values for barrier height of ITO with those of Ti, Mo, Co and Ni, on (100) β-Ga_2O_3 reported by Lyle et al,[42] plotted vs metal work function. The theoretical value from the Mott-Schottky equation is also given, assuming an electron affinity of 4.05 eV.

Figure 6. Reverse J-V characteristics as a function of temperature for ITO Schottky contacts on (100) β-Ga_2O_3. The diameter of each diode is 500 μm.

Figure 7. On/off ratio of or ITO Schottky contacts on (100) β-Ga_2O_3.The devices were measured at -1V forward basis and then the reverse bias shown on the x-axis.

Figure 8. Experimental data for reverse current density characteristics at 400-600K and fit to an $I \propto V^n$ relationship.

Figure 9. Optical microscope image of fully transparent, vertical geometry Ga_2O_3 rectifier employing ITO contacts on both sides. The structure is ITO top Schottky contact, epi Ga_2O_3, Ga_2O_3 substrate and ITO rear Ohmic contact. On the top lightly doped drift layer, the ITO is rectifying, while on the bottom surface of the heavily doped substrate, it is Ohmic after an anneal. The contact pattern is the same as in Figure 2.

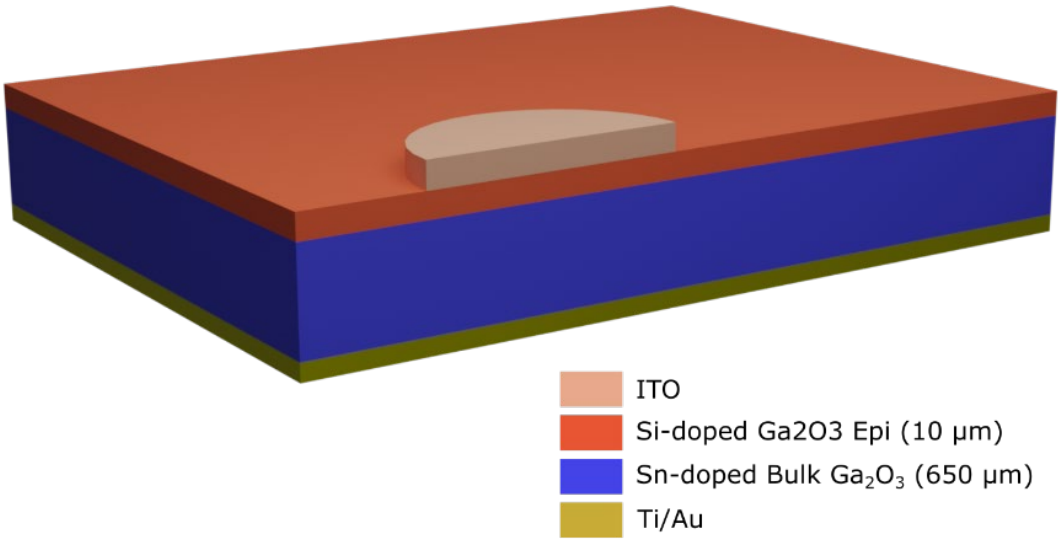
ITO
Si-doped Ga2O3 Epi (10 μm)
Sn-doped Bulk Ga_2O_3 (650 μm)
Ti/Au

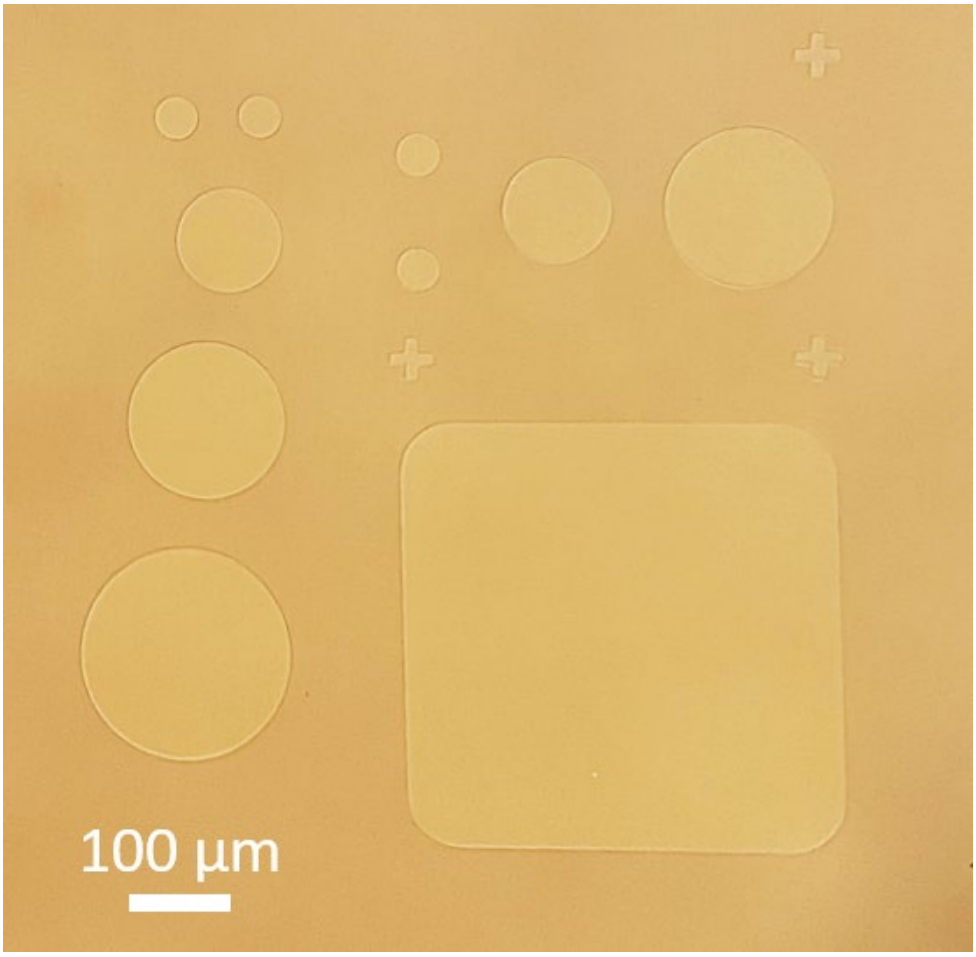
100 µm

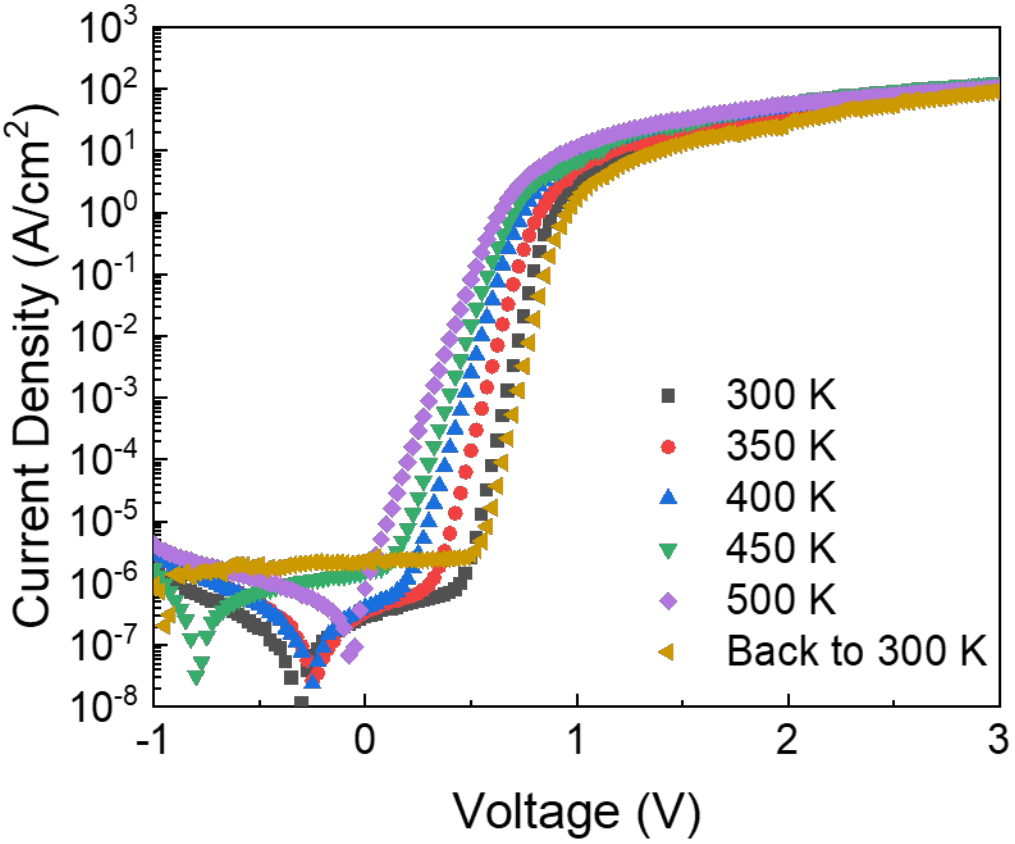
Current Density (A/cm^2)
10^3
10^2
10^1
10^0
10^{-1}
10^{-2}
10^{-3}
10^{-4}
10^{-5}
10^{-6}
10^{-7}
10^{-8}
-1
0
1
2
3
Voltage (V)
300 K
350 K
400 K
450 K
500 K
Back to 300 K

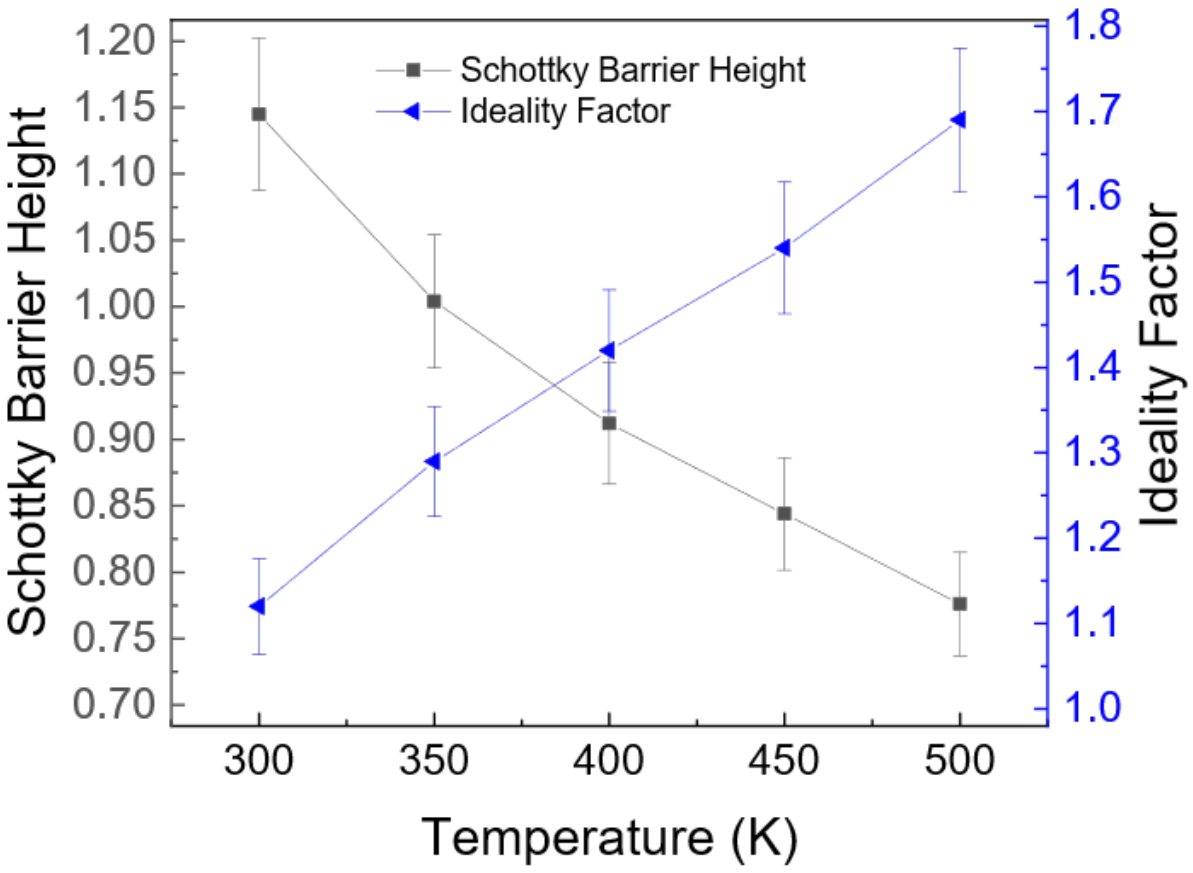
Schottky Barrier Height
Ideality Factor
Schottky Barrier Height
Ideality Factor
Temperature (K)
1.20
1.15
1.10
1.05
1.00
0.95
0.90
0.85
0.80
0.75
0.70
1.8
1.7
1.6
1.5
1.4
1.3
1.2
1.1
1.0
300
350
400
450
500

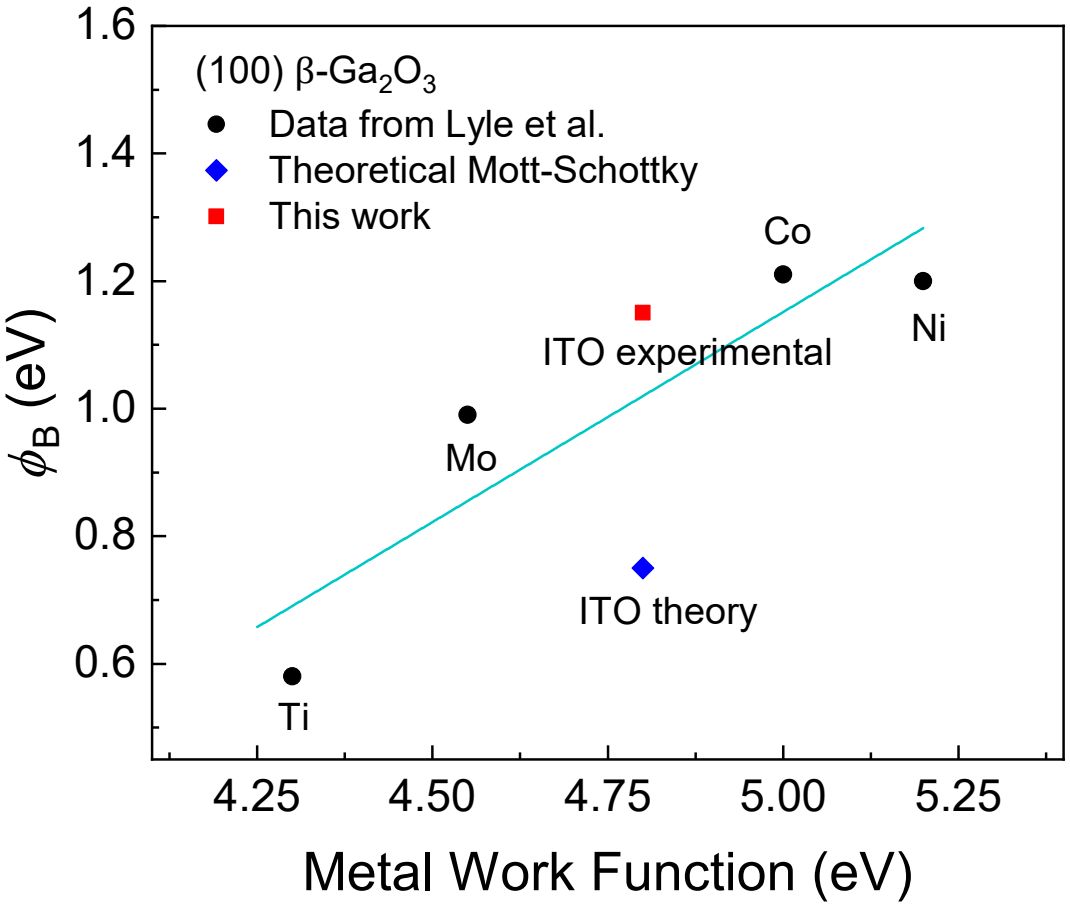
(100) β-Ga2O3
Data from Lyle et al.
Theoretical Mott-Schottky
This work
Co
Ni
ITO experimental
Mo
ITO theory
Ti
1.6
1.4
1.2
1.0
0.8
0.6
ϕB (eV)
4.25
4.50
4.75
5.00
5.25
Metal Work Function (eV)

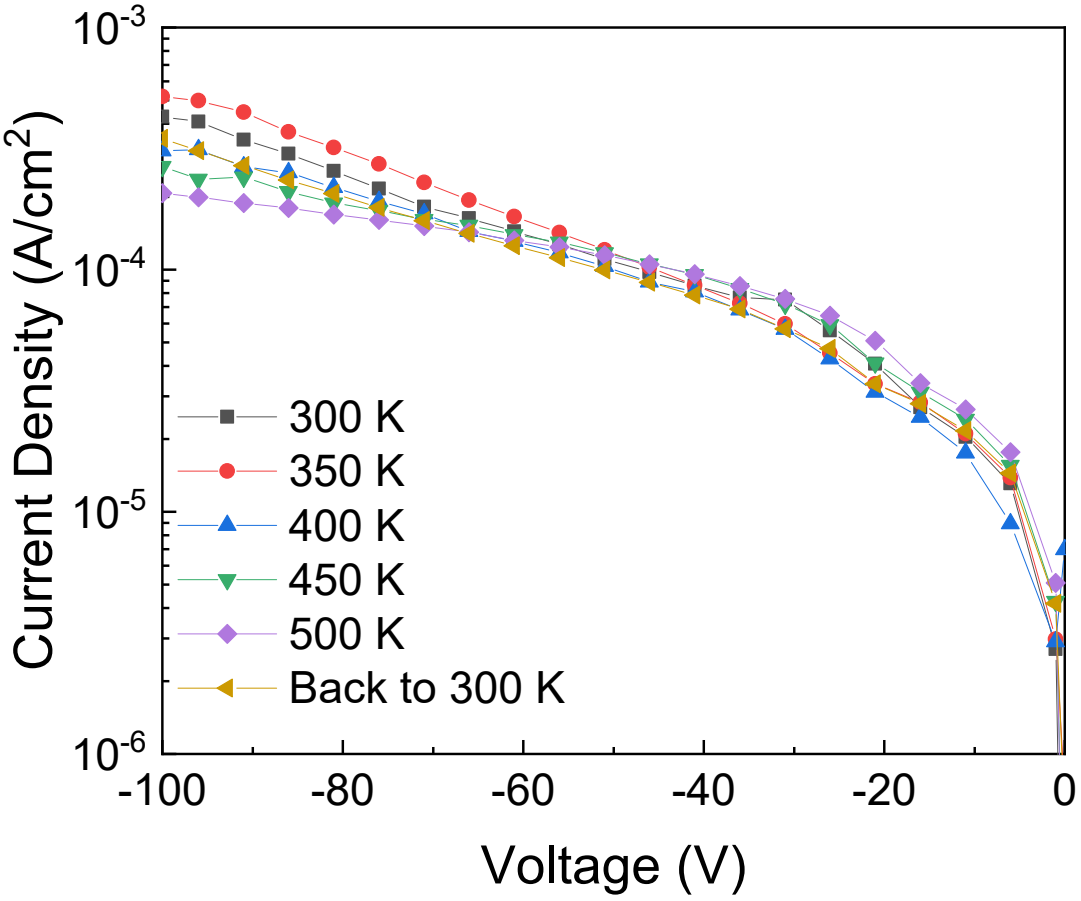
Current Density (A/cm^2)
10^{-3}
10^{-4}
10^{-5}
10^{-6}
300 K
350 K
400 K
450 K
500 K
Back to 300 K
-100
-80
-60
-40
-20
0
Voltage (V)

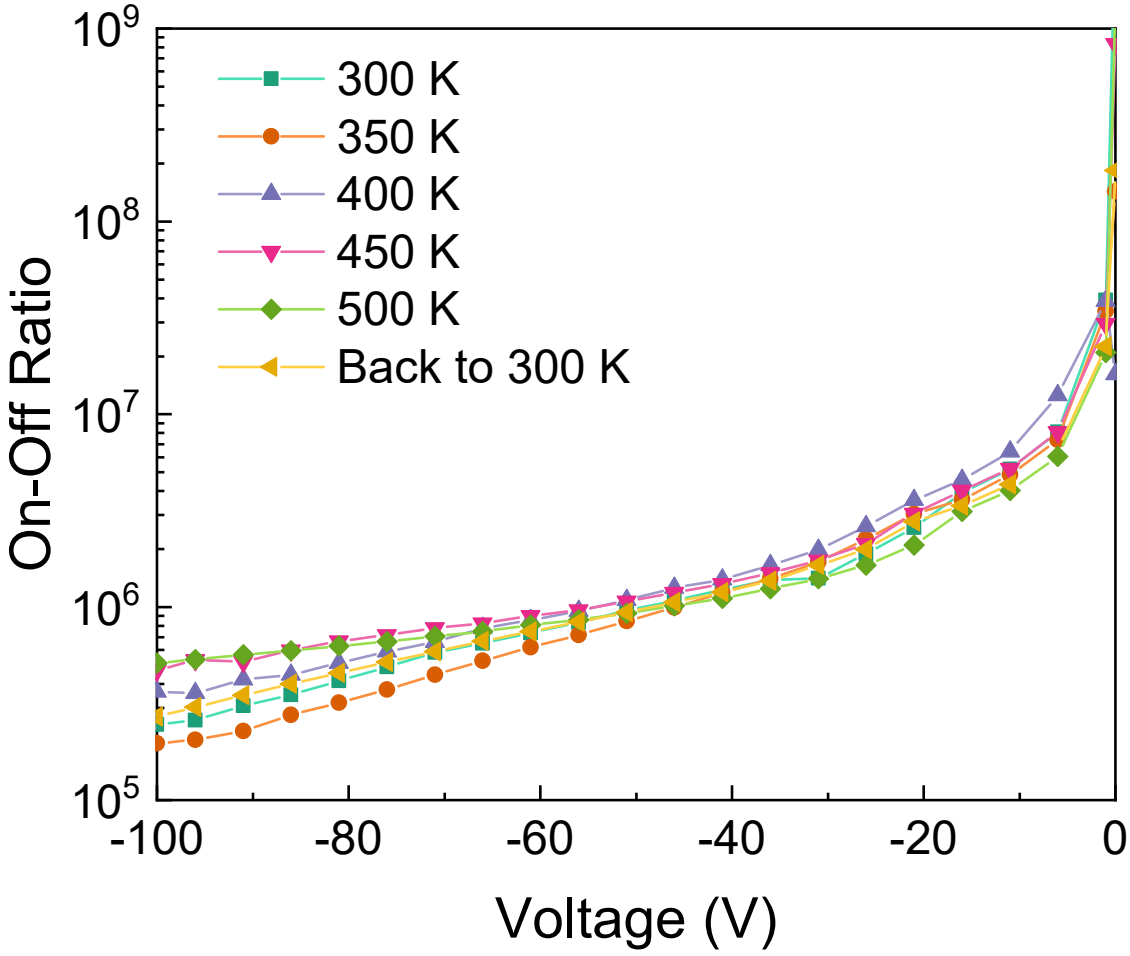
On-Off Ratio
10^9
10^8
10^7
10^6
10^5
300 K
350 K
400 K
450 K
500 K
Back to 300 K
-100
-80
-60
-40
-20
0
Voltage (V)

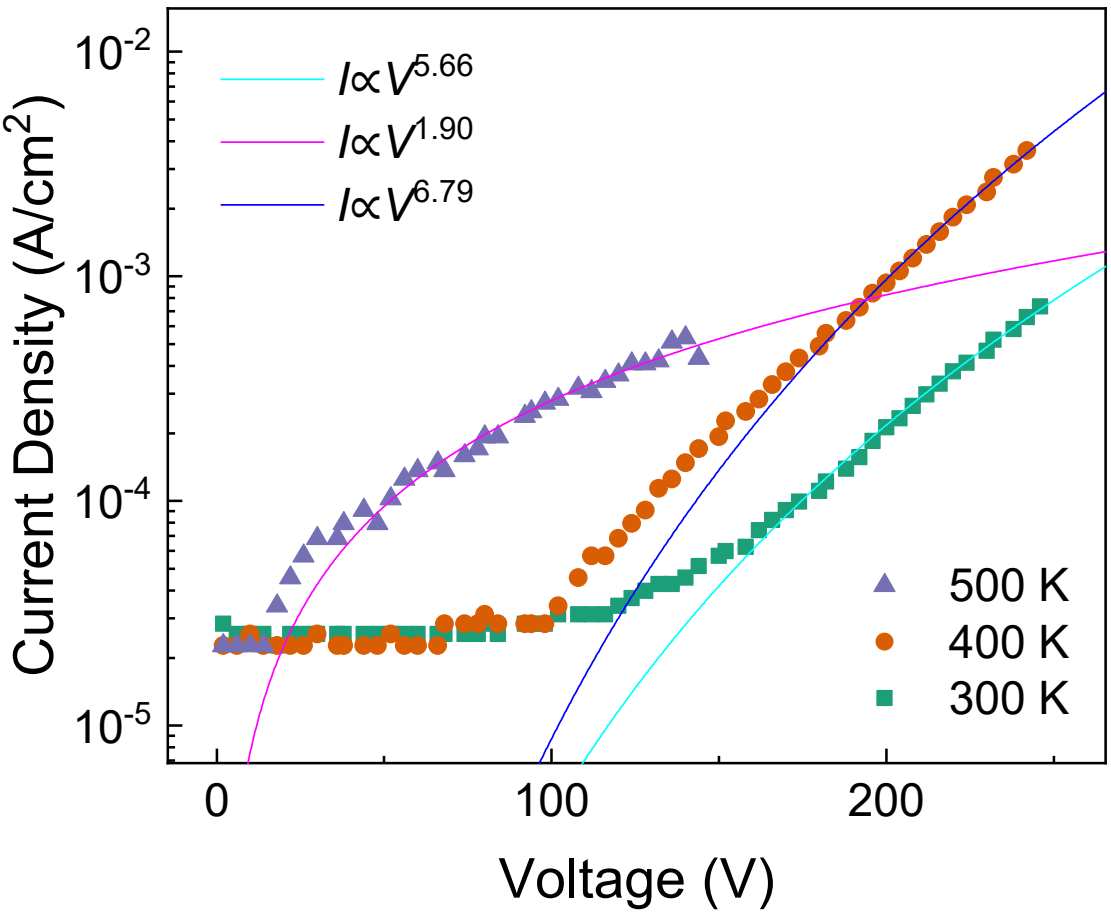
Current Density (A/cm^2)
10^{-2}
10^{-3}
10^{-4}
10^{-5}
$I \propto V^{5.66}$
$I \propto V^{1.90}$
$I \propto V^{6.79}$
500 K
400 K
300 K
0
100
200
Voltage (V)